

Original article

# <sup>99m</sup>Tc glucarate high-resolution imaging of drug sensitive and drug resistant human breast cancer xenografts in SCID mice

Zhonglin Liu<sup>a</sup>, Gail D. Stevenson<sup>a</sup>, Harrison H. Barrett<sup>a</sup>, George A. Kastis<sup>a</sup>, Michel Bettan<sup>a</sup>, Lars R. Furenlid<sup>a</sup>, Donald W. Wilson<sup>a</sup>, James M. Woolfenden<sup>a</sup> and Koon Yan Pak<sup>b</sup>

**Background and aim** Previous studies have showed that <sup>99m</sup>Tc labelled glucarate (GLA) might be an agent for non-invasive detection of breast tumours. In xenografted BT20 breast tumours, GLA was found to have higher uptake than <sup>99m</sup>Tc sestamibi (MIBI). It is unclear whether GLA can localize in all cell line breast cancer xenografts, as well as breast tumours with multidrug resistance (MDR). The present study aimed to investigate the properties of GLA in detecting drug sensitive and drug resistant MCF7 breast cancer xenografts in mice by using dynamic single photon emission computed tomography (SPECT) imaging.

**Methods** MCF7/S cells are drug sensitive breast carcinoma cells. MCF7/D40 cells are 40-fold more resistant to doxorubicin compared to MCF7/S. Subcutaneous tumours were grown in SCID mice for 10–14 days after injection of 1 × 10<sup>6</sup> cells into the right thigh. Anaesthetized mice with MCF7/S (MIBI, n=9; GLA, n=8) and MCF7/D40 (MIBI, n=6; GLA, n=5) tumours were imaged using a high-resolution SPECT system called FASTSPECT. Dynamic images were acquired for 2 h after intravenous injection of GLA or MIBI. Expression of MDR P-glycoprotein (Pgp) in the tumours was demonstrated in the MCF7/D40 tumours by western blotting, not in the MCF7/S tumours.

**Results** The xenografted tumours were visualized unequivocally within 10–30 min in GLA images and

remained detectable for at least 2 h after injection. Drug resistant tumours, from which MIBI was rapidly expelled, retained GLA as readily as did drug sensitive tumours. The biodistribution data of GLA demonstrated significantly higher accumulation (%ID/g) compared to MIBI.

**Conclusion** MCF7 tumour xenografts can be detected by <sup>99m</sup>Tc glucarate imaging. More importantly, <sup>99m</sup>Tc glucarate can potentially localize drug resistant breast tumours. *Nucl Med Commun* 25:711–720  
© 2004 Lippincott Williams & Wilkins.

Nuclear Medicine Communications 2004, 25:711–720

**Keywords:** <sup>99m</sup>Tc glucarate, <sup>99m</sup>Tc sestamibi, breast cancer, multidrug resistant, SCID mice, high-resolution SPECT

<sup>a</sup>Department of Radiology, The University of Arizona, Tucson, Arizona and <sup>b</sup>Molecular Targeting Technologies Inc., West Chester, Philadelphia, USA.

Supported by NIH grants P41 EB002035 and R24CA83148.

Correspondence to Dr Zhonglin Liu, Department of Radiology, The University of Arizona, P.O. Box 245067, Tucson, AZ 85724-5067, USA.  
Tel: +1 520 626 4248; fax: +1 520 626 2892;  
e-mail: zliu@radiology.arizona.edu

Received 17 November 2003 Accepted 16 January 2004

## Introduction

Scintimammography (SMM) is an adjunct to conventional mammography in identifying patients with breast cancer using several radiopharmaceuticals either currently available or still under investigation [1–8]. <sup>99m</sup>Tc sestamibi (MIBI) scintimammography has been shown to have clinical utility in identifying breast tumours that are difficult to study with conventional mammography [1–3]. It has been approved by the U.S. Food and Drug Administration as an adjunct to mammography in the detection of breast cancer. Compared to conventional mammography, <sup>99m</sup>Tc sestamibi imaging has superior utility in patients with large amounts of glandular tissue and dense breasts [9–11].

<sup>99m</sup>Tc sestamibi is a lipophilic monocationic radiotracer that accumulates predominantly within the mitochondria

and cytoplasm of cells on the basis electrical potentials generated across membrane bilayers. Overall institutional sensitivity and specificity in <sup>99m</sup>Tc sestamibi imaging are 75.4% and 82.7% for breast cancer detection [3]. The positive predictive value is 74.5% and the negative predictive value is 83.4%. Perhaps because of either poor gamma camera resolution or lower <sup>99m</sup>Tc sestamibi uptake in the tumours, the sensitivity of <sup>99m</sup>Tc sestamibi SMM for small lesions is not as good as it is in larger lesions. For example, the sensitivity for tumours under 1 cm in size was only 48.2% [3]. Larger lesions may also be undetected by <sup>99m</sup>Tc sestamibi SMM due to low cellular proliferation or overexpression of a multidrug resistance (MDR) gene, MDR1, which encodes for a membrane glycoprotein, P-glycoprotein (Pgp) [12]. Pgp acts as an energy dependent drug-efflux pump and allows transport of a wide range of structurally and functionally

unrelated cytotoxic drugs out of tumour cells [13,14]. In addition to the drugs, many surrogate markers of Pgp function *in vivo* such as  $^{99m}\text{Tc}$  sestamibi can also be pumped out [15,16]. Faster clearance of  $^{99m}\text{Tc}$  sestamibi has been observed in tumours that express Pgp compared with tumours that do not [17]. Consequently, there is a need for an alternative marker that is not as readily eliminated by Pgp.

D-glucuronic acid is a six-carbon dicarboxylic acid sugar and a natural catabolite of glucuronic acid metabolism in mammals [18,19]. All mammals excrete glucuronic acid (glucuronate) as a physiological end product. Glucuronic acid can be readily radiolabelled with sodium pertechnetate, resulting in  $^{99m}\text{Tc}$  glucuronate (GLA), which was originally designed for detecting early necrosis of the heart and brain [19–21]. It was reported that  $^{99m}\text{Tc}$  glucuronate could also concentrate in malignant breast tumours [7,8]. Biodistribution studies indicated that primary breast tumours in patients were visualized at early imaging time with  $^{99m}\text{Tc}$  glucuronate [22]. In SCID mice with xenografted BT20 tumours,  $^{99m}\text{Tc}$  glucuronate was found to have significantly higher uptake than  $^{99m}\text{Tc}$  sestamibi [7]. The mechanisms of  $^{99m}\text{Tc}$  glucuronate uptake and accumulation in the breast tumours are as yet unknown. It is unclear if  $^{99m}\text{Tc}$  glucuronate will localize in all cell line breast cancer xenografts.

The purpose of this study was to determine the properties of  $^{99m}\text{Tc}$  glucuronate in detecting and localizing human MCF-7 breast cancer xenografts including drug sensitive and drug resistant breast tumours. We compared the *in vivo* kinetics of  $^{99m}\text{Tc}$  glucuronate with  $^{99m}\text{Tc}$  sestamibi in SCID mice using high-resolution SPECT imaging. In addition to studying the properties of  $^{99m}\text{Tc}$  glucuronate, we wanted to clarify whether a novel high-resolution stationary single photon emission computed tomography (SPECT) system, FASTSPECT, would yield high-resolution images combined with the capability of fast dynamic imaging for radiopharmaceutical kinetic study in a mouse tumour model.

## Materials and methods

### Tumour cell lines

Drug sensitive cell lines (MCF7/S) were doxorubicin sensitive MCF7 breast carcinoma cells originally obtained from the American Type Culture Collection (ATCC #HTB-22, Rockville, MD).

Drug resistant cell lines (MCF7/D40) were generated *in vitro* by successively culturing parental MCF7 cells in slowly increasing concentrations of doxorubicin in a multiple step procedure [23]. Fresh drug was added when the medium was changed three times a week. The concentration of doxorubicin was increased from  $1 \times 10^{-8}$  M to  $7 \times 10^{-8}$  M over 19 months. During an additional

12 months, the concentration was increased to  $4 \times 10^{-7}$  M, representing full development of the doxorubicin resistant variant cells. The presence of Pgp in the MCF7/D40 cells was confirmed by immunoblot analysis using the C219 mouse monoclonal antibody (IgG) with  $^{125}\text{I}$  labelled rabbit anti-mouse IgG as the secondary antibody. The drug resistant cells were maintained in a drug-free medium for 1 week prior to experiments.

### Tumour models

Severe combined immunodeficient (SCID) mice weighing 18–22 g were obtained from the SCID mouse core facility at the University of Arizona Comprehensive Cancer Center. Mice were housed under pathogen-free conditions in microisolator cages with laboratory chow and water available. Subcutaneous breast adenocarcinomas were established by injecting  $9 \times 10^6$  MCF7 cells into the mouse right thigh. The volume of tumour was monitored and measured daily. After 14 days, tumours reached a size of 200–500 mm<sup>3</sup> for imaging.

Animals were anaesthetized with 1.0–1.5% isoflurane, and the jugular vein was catheterized with a PE10 catheter via a surgical procedure. The catheter was secured proximal to the opening with a ligature, and further secured distal to the opening with a second ligature.

### Experimental groups

#### MCF7/S tumour model

A total of 17 SCID mice with drug sensitive tumours were studied. FASTSPECT imaging was performed in nine mice with  $^{99m}\text{Tc}$  sestamibi (MIBI/S group), eight with  $^{99m}\text{Tc}$  glucuronate (GLA/S group).

#### MCF7/D40 tumour model

There were 11 mice with drug resistant tumours subjected to FASTSPECT imaging. The images were obtained in six mice with  $^{99m}\text{Tc}$  sestamibi (MIBI/D40 group), five with  $^{99m}\text{Tc}$  glucuronate (GLA/D40 group).

### Preparation of the radiopharmaceutical

Glucuronate kits were provided by Molecular Targeting Technologies, Inc., (West Chester, PA) as single-vial doses containing 12.5 mg of glucuronate. The reagent in the vial was a sterile, non-pyrogenic, lyophilized composition of stannous chloride, glucuronate, sodium bicarbonate and hydrochloric acid. One millilitre of  $^{99m}\text{Tc}$  as sodium pertechnetate (not less than 2.59 GBq (70 mCi)) was added to the vial and allowed to react at room temperature for 15 min. The radiochemical purity (RCP) of the  $^{99m}\text{Tc}$  glucuronate was determined by Gelman instant thin-layer silica gel (ITLC-SG) strips developed in saline and acetone. In the ITLC-SG strip developed by saline,  $^{99m}\text{Tc}$  colloid remained at the origin while  $^{99m}\text{Tc}$  glucuronate and [ $^{99m}\text{Tc}$ ]pertechnetate migrated near the solvent front. In the strip developed by acetone,  $^{99m}\text{Tc}$  glucuronate and  $^{99m}\text{Tc}$  colloid remained at the origin

while [<sup>99m</sup>Tc]pertechnetate moved near the solvent front. The RCP of <sup>99m</sup>Tc GLA was greater than 95% for all experimental injections. <sup>99m</sup>Tc glucarate was used within 3 h after preparation.

<sup>99m</sup>Tc sestamibi was prepared with a Cardiolite kit (Bristol-Myers Squibb) provided by Syncor Corporation. The RCP was greater than 95%.

#### Acquisition of high-resolution SPECT images

Dynamic SPECT images were acquired using a high-resolution stationary SPECT system, FASTSPECT, which consists of 24 small modular gamma cameras and a cylindrical aperture [24,25]. The system was built at the Radiology Research Laboratory of the University of Arizona. Twenty-four 1 mm diameter pinholes were drilled in the aperture such that a point source in the centre of the field of view simultaneously is projected to the centre of each camera. The total magnification is 3.5 in a 3.0 cm × 3.2 cm × 3.2 cm field of view. The spatial resolution of the system in the reconstructed image is about 1.0 mm in all directions. Point source sensitivity in air is 359.5 cps/MBq (13.3 cps/μCi).

Anaesthetized animals were placed inside the FASTSPECT aperture using a translation stage. <sup>99m</sup>Tc sestamibi or <sup>99m</sup>Tc glucarate (0.15 ml, 111–222 MBq (3–6 mCi)) was injected via the jugular vein catheter followed by a 0.08 ml saline flush. Beginning immediately upon injection, dynamic images were acquired every 1 min for the first 10 min, followed by 5 min acquisitions at 15, 20 and 30 min. Then 5 min images were obtained every 15 min from 30 to 120 min after injection. Twenty-four projections, one from each camera, were generated using a look-up-table scheme. In this scheme, each scintillation event within the camera's NaI crystal was registered as the digitized outputs from the camera's four photomultiplier tubes. In order to estimate energy and interaction position, the four outputs were then compared to a 20-bit look-up table. This table was precalculated using a calibration procedure that involved moving a collimated source across the camera face.

#### Image processing

The maximum likelihood expectation maximization (MLEM) reconstruction algorithm was applied to generate 3-dimensional images. All images were reconstructed using 100 iterations. The projection model built into this algorithm was generated using a calibration scheme that involved moving an uncollimated source through the imaging system's field of view in 1 mm steps and recording the system response at each calibration point. Using the software of SlicerDicer (PIXOTEC LLC, Renton, WA), transaxial, coronal and sagittal slices of the tumour were generated with 1 pixel

thickness (1.0 mm). A lower threshold value was set around 60 in a colour range from 0 to 255 to display the uptake of <sup>99m</sup>Tc glucarate or <sup>99m</sup>Tc sestamibi in the tumour.

In all the images from 1 to 120 min after injection, regions of interest (ROIs) over the tumours were created from one coronal slice with the highest accumulation of <sup>99m</sup>Tc glucarate or <sup>99m</sup>Tc sestamibi. An ROI was also created over a non-tumour area to determine the radioactivity of background. After correction for the background and radioactive decay, the radioactivity in the tumour was projected onto the dynamic images for determinations of time-activity curve.

#### Biodistribution measurements

After images were acquired, the mice were killed with a lethal dose of barbiturate. Blood samples, tumour, skeletal muscle, heart, lung, kidney and liver were harvested. The tissue samples were weighed and measured using a CRC-4 Radioisotope Dose Calibrator (Capintec, Ramsey, NJ). The radioactivity in the tissue samples was expressed as percentage of injected dose per gram tissue (%ID/g). The samples were counted in a well counter adjusted to the <sup>99m</sup>Tc window if the radioactivity was lower than 74 kBq (2.0 μCi). Standards prepared from an aliquot of the administered <sup>99m</sup>Tc glucarate source were counted at the same time to convert the counts per minute from the gamma well counter into kilobecquerels or microcuries.

#### Western blot analysis

In order to determine the drug resistant properties in the xenografted tumours, western blot analysis was applied to detect Pgp expression. The tumour samples were frozen in liquid nitrogen for more than 3 days. Randomly selected MCF7/S and MCF7/D40 tumour tissues were homogenized in lysis buffer after <sup>99m</sup>Tc decayed to background level. Protein concentration was determined using a BioRad DC (BioRad, Hercules, CA) protein assay. A total of 100 mg protein was loaded per lane on a 10% SDS-PAGE gel. Completed gel was then transferred to a PVDF membrane and probed with a mouse monoclonal antibody C219 (1:200 dilution) against Pgp (Signet, Dedham, MA). A rabbit anti-mouse HRP secondary antibody was used (Santa Cruz Biotechnology, Inc., Santa Cruz, CA), and detected with an ECL western blot analysis system (Amersham, Piscataway, NJ).

#### Data analysis

All results were expressed as mean ± SEM. Comparisons between groups were performed with one-way analysis of variance. Comparisons between two variables within a group were made by means of the two-tailed paired *t*-test. Probability values less than 0.05 were considered significant.

Individual  $^{99m}\text{Tc}$  glucarate and  $^{99m}\text{Tc}$  sestamibi clearance curves from the peak uptake were fit using non-linear regression procedures available in TableCurve 2D software (Systat Software Inc., Richmond, CA).

### Ethics

All experiments were performed in accordance with the guidelines for animal research from the National Institutes of Health (NIH publication 85-23, revised 1985) and were approved by the Institutional Animal Care and Use Committee (IACUC) at the University of Arizona.

## Results

### Pgp expression

Western blot analysis indicated that human MDR1 Pgp was well expressed in the xenografted MCF7/D40 tumours. A prominent band was observed in tumour cell membrane preparations with C219 antibody, indicating Pgp expression in the MCF7/D40 tumour samples. No immunodetectable MDR1 Pgp was presented in the xenografted MCF7/S tumour samples.

### FASTSPECT tumour imaging

All tumours of  $^{99m}\text{Tc}$  glucarate groups were initially visualized within 5 min by FASTSPECT imaging after injection of  $^{99m}\text{Tc}$  glucarate, and they were unequivocally localized within 10–30 min. Figure 1 shows representative  $^{99m}\text{Tc}$  glucarate coronal tomographic images in a mouse with subcutaneous MCF7/S tumour 20 min post injection. Dynamic  $^{99m}\text{Tc}$  glucarate images demonstrated that the radioactive accumulation in the MCF7 tumours remained for at least 120 min post-injection. Representative dynamic images in MCF7/S and MCF7/D40 are shown in Fig. 2. Relative to the drug sensitive tumours, the drug resistant tumours exhibited the same level uptake of  $^{99m}\text{Tc}$  glucarate during the entire period for dynamic acquisition. Two hours post-administration, the MCF7/D40 tumour xenograft could be well visualized in all directions of tomographic  $^{99m}\text{Tc}$  glucarate images (Fig. 3). In comparison with  $^{99m}\text{Tc}$  sestamibi imaging,  $^{99m}\text{Tc}$  glucarate imaging demonstrated lower background activity and higher tumour accumulation (Figs 2 and 4).

The MCF7/S tumours could be detected initially by FASTSPECT imaging 2–10 min after intravenous administration with  $^{99m}\text{Tc}$  sestamibi. Two hours post-injection, dynamic images demonstrated that tumour activity remained detectable (Figs. 4A and B). In contrast, as shown in Fig. 4(C and D), the MCF7/D40 tumours could be localized only 2–4 min post-injection of  $^{99m}\text{Tc}$  sestamibi; then the radioactivity in the tumours dropped quickly to background levels.

### Kinetics of $^{99m}\text{Tc}$ glucarate and $^{99m}\text{Tc}$ sestamibi in MCF7 tumours

Figure 5 shows time–activity curves plotted from 1 min to 120 min for  $^{99m}\text{Tc}$  glucarate and  $^{99m}\text{Tc}$  sestamibi in the

MCF7/S and MCF7/D40 xenografts determined by the computerized ROI analysis of FASTSPECT images that were background subtracted and decay corrected. The time–activity curves of  $^{99m}\text{Tc}$  sestamibi were significantly lower for the MCF7/D40 tumours than for the MCF7/S tumours at each point in time from 5 min to 120 min. There was no such difference at each point between the  $^{99m}\text{Tc}$  glucarate time–activity curves of the MCF7/S and MCF7/D40 tumours. There was significantly higher peak uptake and end radioactivity for  $^{99m}\text{Tc}$  glucarate than for  $^{99m}\text{Tc}$  sestamibi in each xenografted tumour model ( $P < 0.05$ ; Fig. 6).

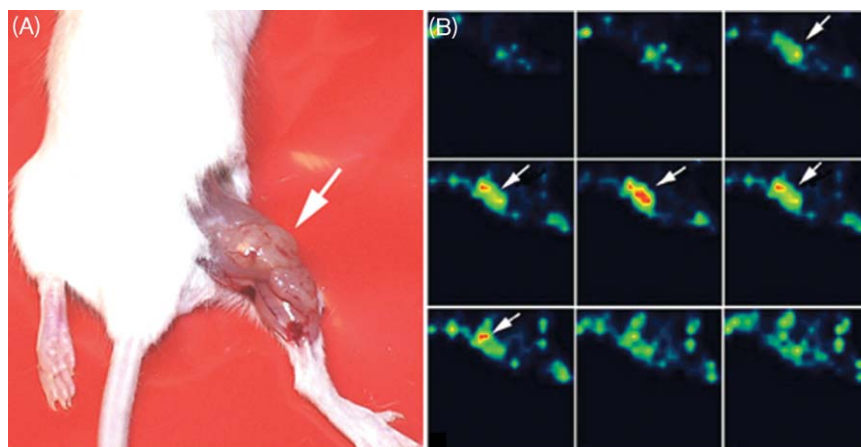
Clearance of  $^{99m}\text{Tc}$  glucarate plotted as the percentage of peak activity did not differ significantly in the MCF7/D40 tumours compared with MCF7/S. In contrast, the clearance of  $^{99m}\text{Tc}$  sestamibi was greater in MCF7/D40 tumours (Fig. 7). Both  $^{99m}\text{Tc}$  glucarate and  $^{99m}\text{Tc}$  sestamibi exhibited biphasic clearance curves, and biexponential equations were found to provide the best fits to the curves. The early phase showed fast clearance and the late phase showed slow clearance. The half-time values (minutes) of biexponential washout ( $T_{1/2}$ , time to reach half of initial activity) from the tumours are shown in Table 1. The  $T_{1/2}$  values were significantly lower for MCF7/D40 than for MCF7/S during both the early and late phases with  $^{99m}\text{Tc}$  sestamibi ( $P < 0.05$ ). With  $^{99m}\text{Tc}$  glucarate, however, there was no difference in  $T_{1/2}$  values between MCF7/D40 and MCF7/S.  $^{99m}\text{Tc}$  glucarate had a significantly shorter  $T_{1/2}$  in the late phase compared to  $^{99m}\text{Tc}$  sestamibi in MCF7/S.  $^{99m}\text{Tc}$  sestamibi in the MCF7/D40 tumours exhibited shorter  $T_{1/2}$  than  $^{99m}\text{Tc}$  glucarate in the early phase ( $P < 0.05$ ).

The 2 h fractional washout (percent peak activity) of  $^{99m}\text{Tc}$  sestamibi was significantly greater in MCF7/D40 than that in MCF7/S ( $71.7 \pm 1.7\%$  vs  $50.2 \pm 5.3\%$ ,  $P < 0.05$ ), but there was no difference ( $71.9 \pm 2.9\%$  vs  $72.8 \pm 3.1\%$ ,  $P > 0.05$ ) for  $^{99m}\text{Tc}$  glucarate.

### Biodistribution data

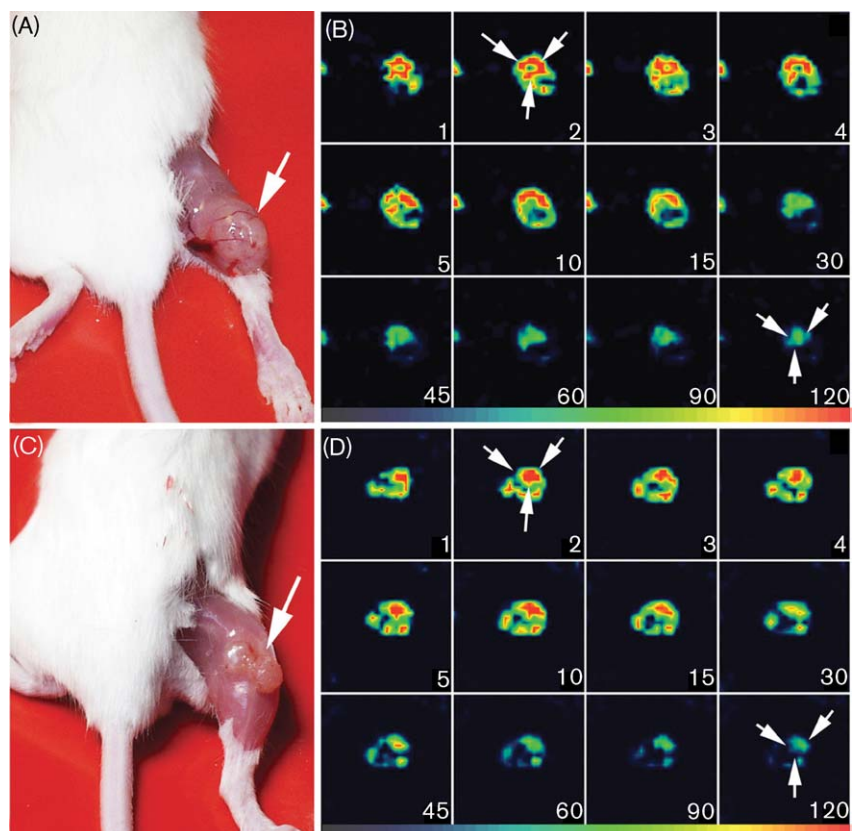
The average tumour weight for the 28 mice was  $0.12 \pm 0.02$  g. No difference was found in tumour weight between the MCF7/S and MCF7/D40 tumours imaged with  $^{99m}\text{Tc}$  glucarate or  $^{99m}\text{Tc}$  sestamibi. The biodistribution data are shown in Table 2.  $^{99m}\text{Tc}$  sestamibi exhibited significantly lower radioactive accumulation (%ID/g) in the MCF7/D40 tumours than that in the MCF7/S tumours, ( $P < 0.05$ ).  $^{99m}\text{Tc}$  glucarate showed significantly higher accumulation (%ID/g) than  $^{99m}\text{Tc}$  sestamibi in either the MCF7/S or MCF/D40 tumours. There was no difference in  $^{99m}\text{Tc}$  glucarate accumulations between the two kinds of xenografted tumour models.  $^{99m}\text{Tc}$  glucarate demonstrated significantly lower radioactivity in non-tumour soft tissue (muscle) compared to  $^{99m}\text{Tc}$  sestamibi ( $P < 0.05$ ). As a result, 2 h after injection, the

**Fig. 1**



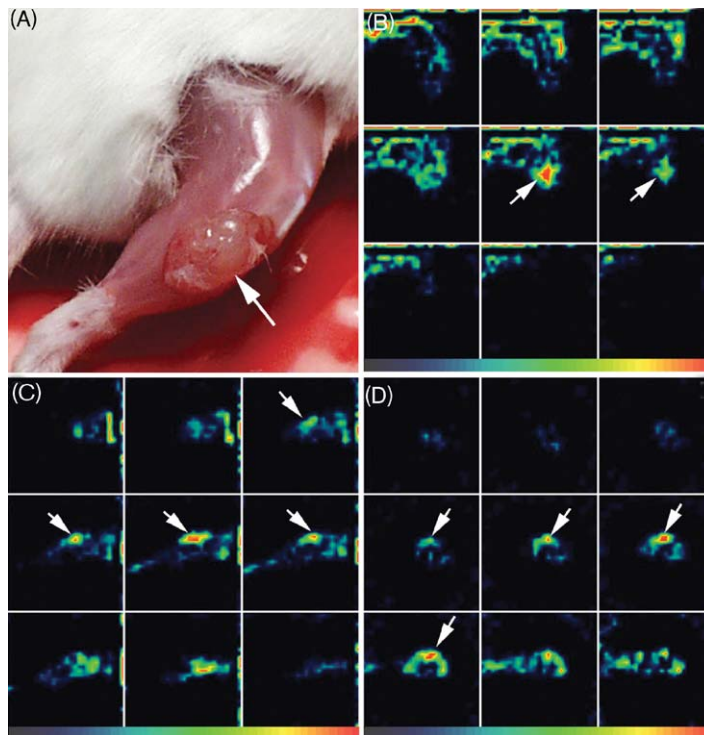
$^{99m}\text{Tc}$  glucarate FASTSPECT coronal images (right panel) in a mouse with MCF7/S tumour xenograft on right thigh (left panel) 20 min after injection. Tumour (arrow) was localized clearly with low radioactive background on  $^{99m}\text{Tc}$  glucarate images.

**Fig. 2**



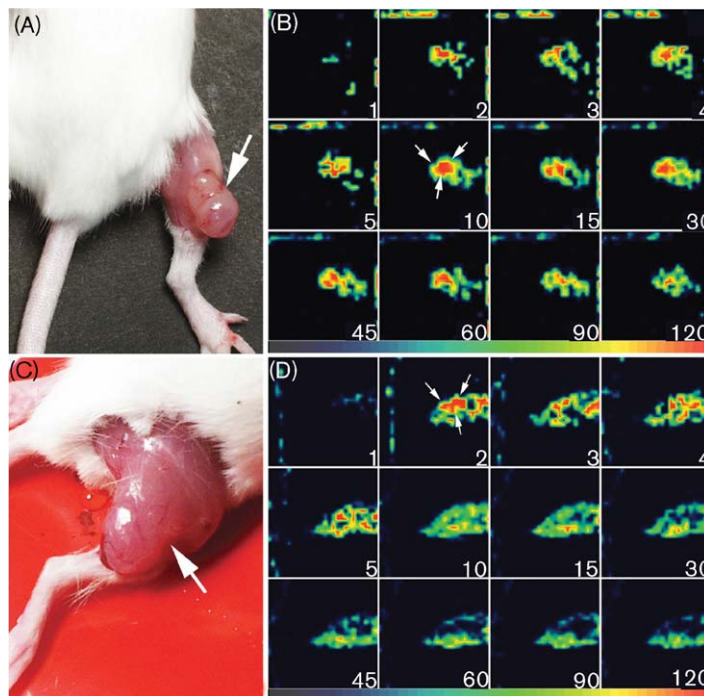
(A and B)  $^{99m}\text{Tc}$  glucarate dynamic FASTSPECT images (serial transaxial slices) from a mouse with MCF7/S breast tumour (arrow). The tumour (arrow) was visualized within 5 min and stayed well-defined for at least 120 min after  $^{99m}\text{Tc}$  glucarate injection. The time after injection is shown in the lower right corner of each image. (C and D)  $^{99m}\text{Tc}$  glucarate dynamic FASTSPECT images (serial transaxial slices) from a mouse with MCF7/D40 breast tumour (arrow). The tumour (arrow) was visualized during the period for dynamic acquisition as well as in the MCF7/S tumour above.

Fig. 3



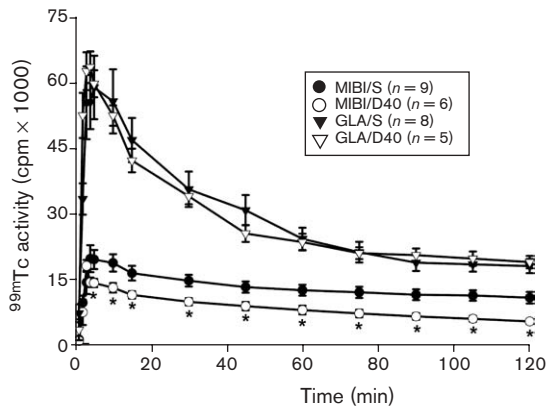
<sup>99m</sup>Tc glucurate FASTSPECT images 120 min after injection in a mouse with MCF7/D40 tumour xenograft on right thigh (A). Tumour (arrow) was well localized in all directions of tomographic images (B: coronal; C: sagittal; D: transaxial slices).

Fig. 4



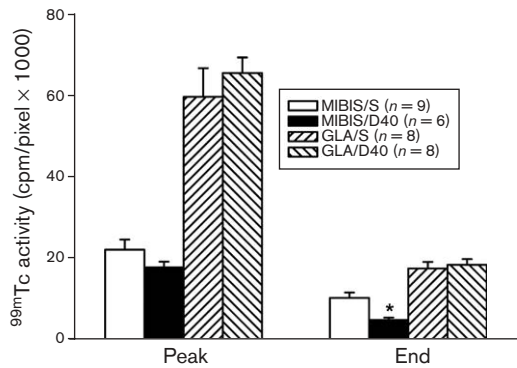
(A and B) Dynamic FASTSPECT images from a mouse with MCF7/S breast tumour on right thigh (arrow) using <sup>99m</sup>Tc sestamibi (serial sagittal slices). The tumour was unequivocally visualized after about 10 min and remained detectable until 120 min after injection. (C and D) <sup>99m</sup>Tc sestamibi dynamic FASTSPECT images from a mouse with MCF7/D40 tumour xenograft on right thigh (serial sagittal slices). The tumour was visualized only 2–4 min after injection. The tumour radioactivity dropped quickly to the background level.

**Fig. 5**



Time-activity curves of <sup>99m</sup>Tc sestamibi and <sup>99m</sup>Tc glucarate in the MCF7/S and MCF7/D40 tumours. The radioactivity in both tumour models with <sup>99m</sup>Tc glucarate was significantly higher at all points than with <sup>99m</sup>Tc sestamibi. In contrast to <sup>99m</sup>Tc sestamibi, the radioactivity from <sup>99m</sup>Tc glucarate was not considerably lower in MCF7/D40 than in MCF7/S tumours. MIBI, <sup>99m</sup>Tc sestamibi; GLA, <sup>99m</sup>Tc glucarate; S, MCF7/S; D40, MCF7/D40; \**P*<0.05 compared to MIBI/S. Error bar=SEM.

**Fig. 6**



The peak uptake and end radioactivity detected by FASTSPECT imaging using <sup>99m</sup>Tc glucarate were significantly higher than that using <sup>99m</sup>Tc sestamibi in both of the MCF7/S and MCF7/D40 tumours. The end activity of <sup>99m</sup>Tc sestamibi in the MCF7/D40 tumours was significantly lower than that in the MCF7/S tumours. Abbreviations as in Fig. 5. \**P*<0.05 compared to MIBI/S.

tumour-to-muscle ratios (tumour/muscle) for <sup>99m</sup>Tc glucarate were 9.4-fold higher than for <sup>99m</sup>Tc sestamibi in the MCF7/S tumours and 19.2-fold higher than in the MCF7/D40 tumours. The blood activity of <sup>99m</sup>Tc sestamibi was significantly lower than <sup>99m</sup>Tc glucarate. Relative to <sup>99m</sup>Tc sestamibi, <sup>99m</sup>Tc glucarate showed a significant lower accumulation in liver.

**Discussion**

In this study, the feasibility of <sup>99m</sup>Tc labelled glucarate for detecting MCF7 breast tumours was assessed and

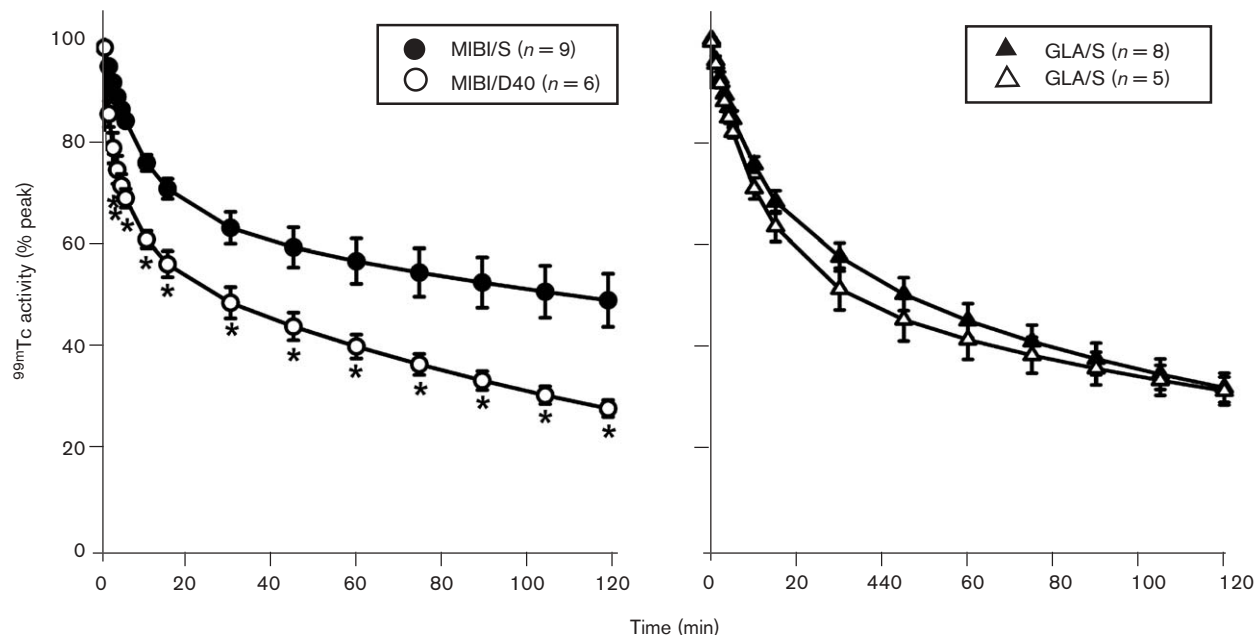
compared to <sup>99m</sup>Tc sestamibi imaging using the high-resolution SPECT system, FASTSPECT. In the xenografted tumour models, <sup>99m</sup>Tc glucarate showed higher tumour uptake than <sup>99m</sup>Tc sestamibi. As described previously, <sup>99m</sup>Tc sestamibi was demonstrated to be a substrate for MDR in the drug resistant MCF7 tumours. The expression of Pgp is responsible for the high washout rate of <sup>99m</sup>Tc sestamibi. <sup>99m</sup>Tc glucarate, in contrast, exhibited the same kinetics in the drug resistant tumours as in the MCF7/S tumours, which are sensitive to doxorubicin. Thus, MDR is not a factor affecting the accumulation of <sup>99m</sup>Tc glucarate in the MCF7 breast tumours.

<sup>99m</sup>Tc sestamibi is an isonitrile compound and is concentrated primarily in mitochondria. The uptake of cationic <sup>99m</sup>Tc sestamibi depends on negative transmembrane and mitochondrial potentials. Although the lipophilic sestamibi might diffuse through plasma membranes by a passive mechanism, Na<sup>+</sup>/K<sup>+</sup> ATPase pump activity is required to maintain the membrane potential [26–29]. <sup>99m</sup>Tc sestamibi is fixed intracellularly as long as the cell membrane integrity is intact and nutrient blood flow persists. This active energy dependent mechanism might explain the slower washout of <sup>99m</sup>Tc sestamibi compared to that of <sup>99m</sup>Tc glucarate from the tumour xenografts in the present study.

Since glucarate is a six-carbon dicarboxylic acid sugar and behaves as a glucose analogue, the increased uptake of GLA may relate to upregulated glucose transport in the tumour cells. Overexpression of glucose transporters directly involves accelerated metabolic processes to accommodate the energy requirements of rapidly dividing cells and provide the carbon backbone for DNA and RNA synthesis for cell proliferation in growing tumours. The uptake of <sup>99m</sup>Tc glucarate in certain cells was inhibited by fructose [20]. Insulin administration was found to increase <sup>99m</sup>Tc glucarate uptakes in the rat hearts, livers and skeletal muscles significantly [30]. These experimental results suggest that <sup>99m</sup>Tc glucarate may enter certain cells by the sugar transport system.

The exact mechanism of <sup>99m</sup>Tc glucarate uptake in tumour is currently unclear. In acute infarcted myocardium, <sup>99m</sup>Tc glucarate was observed to target the nuclei of the necrotic myocardium. High nuclear uptake of <sup>99m</sup>Tc glucarate was also reported in the BT20 human breast tumour cell line [7]; the mitochondrial and cytosolic fractions also sequestered a substantial amount of <sup>99m</sup>Tc glucarate. However, the nuclear fraction of <sup>99m</sup>Tc glucarate distribution in tumour cells was lower than that in infarcted myocytes. When [<sup>14</sup>C]glucarate was administered to rats bearing primary mammary tumours, significant binding of glucarate to proteins was found in the cytosolic fraction [31]. However, it is unclear how

Fig. 7



<sup>99m</sup>Tc glucarate and <sup>99m</sup>Tc sestamibi washout curves from the MCF7/S and MCF7/D40 breast tumours. The radioactivity is plotted as a percentage of the peak activity in the tumour and extended to 2 h using the TableCurve curve-fitting calculation. Abbreviations as in Fig. 5. \*P<0.05 compared to MIBI/S.

Table 1 Biexponential tumour clearance half-time (min)

	<sup>99m</sup> Tc sestamibi		<sup>99m</sup> Tc glucarate	
	MCF7/S	MCF7/D40	MCF7/S	MCF7/D40
Early phase	11.4 ± 1.9	4.4 ± 1.4*	12.2 ± 2.6	12.4 ± 2.3
Late phase	431.3 ± 56.1	178.9 ± 21.5*	170.1 ± 16.2	219.3 ± 38.8

Values are given as the mean ± SEM.

\*P<0.05 compared to MCF7/S.

Table 2 Biodistribution data (%ID/g)

	<sup>99m</sup> Tc sestamibi		<sup>99m</sup> Tc glucarate	
	MCF7/S	MCF7/D40	MCF7/S	MCF7/D40
Blood	0.06 ± 0.01	0.07 ± 0.01*	1.13 ± 0.16**	1.07 ± 0.14**
Muscle	1.37 ± 0.12	1.09 ± 0.32	0.27 ± 0.02**	0.25 ± 0.04**
Lung	0.95 ± 0.16	0.61 ± 0.12	1.08 ± 0.10	1.41 ± 0.54
Heart	10.61 ± 0.89	9.78 ± 1.65	0.64 ± 0.08**	0.55 ± 0.10**
Liver	7.02 ± 1.01	7.67 ± 1.52	2.04 ± 0.37**	1.56 ± 0.18**
Kidneys	21.32 ± 2.03	17.71 ± 3.13	22.70 ± 1.38	22.10 ± 1.59
Tumour	0.64 ± 0.07	0.27 ± 0.05*	1.15 ± 0.17**	1.39 ± 0.12**
Tumour weight (g)	0.12 ± 0.05	0.11 ± 0.04	0.15 ± 0.03	0.10 ± 0.03

Values are given as the mean ± SEM.

\*P<0.05 compared to MCF7/S;

\*\*P<0.05 compared to <sup>99m</sup>Tc sestamibi.

<sup>99m</sup>Tc glucarate is transported into the nuclei and mitochondria. Experimental evidence suggests that the activity of glucarate is mediated via signal transduction pathways involving cAMP and protein kinase C [32]. In acute infarcted myocardium, it is believed that <sup>99m</sup>Tc glucarate is associated with disruption of the myocyte and

nuclear membranes, allowing free intracellular diffusion and electrochemical binding of the negatively charged glucarate complex to positively charged histones. However, the uptake of <sup>99m</sup>Tc glucarate associated with tumour necrosis or membrane breakdown is less likely in the current study, in which we used the xenografted

tumours 10–14 days after tumour implantation. The tumour size was limited to about 0.12 g. No significant tumour necrosis was found in histological and electron microscopic examinations. Under the electron microscope, the tumour cells demonstrated prominent nuclei and abundant mitochondria with no significant breakage (unreported data).

The higher tumour uptake of <sup>99m</sup>Tc glucarate is not simply due to the distribution of the blood pool radioactivity and enhanced tumour vasculature with increased blood supply. Petrov *et al.* observed the tumour blood pool activity in BT20 breast-tumour-bearing SCID mice and compared <sup>99m</sup>Tc glucarate and <sup>99m</sup>Tc-DTPA uptakes [7]. The tumour uptake was significantly greater with <sup>99m</sup>Tc glucarate than with <sup>99m</sup>Tc-DTPA. <sup>99m</sup>Tc-DTPA enabled imaging of the early tumour blood pool soon after injection, but not at 3 h post-injection.

It is not surprising that <sup>99m</sup>Tc sestamibi and <sup>99m</sup>Tc glucarate exhibit different washout kinetics from the xenografted tumour models, as they are chemically different radiopharmaceuticals with different biological pathways. The rapid early clearance phase mainly reflects blood perfusion and effusion, in which the  $T_{1/2}$  values did not differ between <sup>99m</sup>Tc glucarate and <sup>99m</sup>Tc sestamibi in the MCF7/S tumours. The slow second phase, which reflects cellular efflux of radiotracers, showed shorter  $T_{1/2}$  in <sup>99m</sup>Tc glucarate than that in <sup>99m</sup>Tc sestamibi. The greater washout property of <sup>99m</sup>Tc glucarate may be a disadvantage for tumour targeting, but the larger amount of <sup>99m</sup>Tc glucarate radioactivity initially delivered to the tumour might compensate for the greater rate of clearance. Either in early phase or later phase washout of <sup>99m</sup>Tc glucarate, there was no difference in  $T_{1/2}$  between the MCF7/S and MCF7/D40 tumours. This kinetics result in the present study provides evidence that <sup>99m</sup>Tc glucarate is a promising agent in imaging breast tumours, including those with drug resistant properties. The shorter half-time (faster washout) in both of the early and second phase for <sup>99m</sup>Tc sestamibi was observed in the MCF7/D40 tumours compared to the MCF7/S tumours. The faster washout of <sup>99m</sup>Tc sestamibi from the drug resistant tumours can thereby be used as a means of identifying MDR Pgp expression in the patients with breast tumours.

Based on the current data, <sup>99m</sup>Tc glucarate offers favourable characteristics with significantly lower accumulation in non-tumour soft tissue. The mean tumour-to-muscle ratio for <sup>99m</sup>Tc glucarate is 4.5 and 6.2 (9.4 and 19.2 times higher than that for <sup>99m</sup>Tc sestamibi) in both the drug sensitive tumours and drug resistant tumours. In BT20 tumour-bearing mice, Petrov *et al.* reported that the tumour to non-tumour (shoulder region tissue) was 20.53:1 12 h after intravenous injection of <sup>99m</sup>Tc

glucarate. This favourable tumour targeting property of <sup>99m</sup>Tc glucarate may make this agent potentially useful for detecting a small malignant lesion. <sup>99m</sup>Tc sestamibi is not accurate in the detection of axillary lymph node metastasis [33–35], but <sup>99m</sup>Tc glucarate might be superior in the visualization of malignant axillary lymph node. <sup>99m</sup>Tc glucarate may provide utility in visualizing breast tumours and axillary metastases in cases where the MDR1 Pgp is overexpressed or the tumours become resistant to drugs during chemotherapy.

The rapid sequences of tomographic images obtained in this study demonstrate the capability of FASTSPECT for quantitative 3-dimensional imaging. Such functional images are not practical with conventional rotating SPECT systems. FASTSPECT provides an ideal approach for tumour targeting and radiopharmaceutical *in vivo* kinetic studies using small xenografted tumours with less necrosis. It is a dedicated imaging system with stationary camera modules and a stationary multiple pinhole aperture [24,25]. The stationary multiple pinhole collimation overcomes the disadvantages of poor sensitivity and long-time acquisition of projection data in single pinhole or rotating multi-pinhole SPECT cameras, and makes it possible to perform fast dynamic tomographic imaging in small animals. Since no centre-of-rotation corrections are required, artifacts caused by inaccurate centre of rotation are not present in this high-resolution SPECT system.

## Conclusion

The results in this study demonstrate that MCF7 human breast tumour xenografts can be detected by <sup>99m</sup>Tc glucarate *in vivo* imaging with unequivocal visualization within 10–30 min, and remain visible for at least 2 h after intravenous administration. <sup>99m</sup>Tc glucarate offers favourable imaging properties of higher uptake in the MCF7 breast tumours compared to <sup>99m</sup>Tc sestamibi. More importantly, <sup>99m</sup>Tc glucarate can potentially localize drug resistant breast tumours, from which <sup>99m</sup>Tc sestamibi is rapidly expelled by Pgp, a drug-efflux pump. Thus, <sup>99m</sup>Tc glucarate warrants further study to determine its utility in screening for breast cancer, characterizing suspicious lesions, detecting axillary lymph node metastasis and evaluating various antitumour therapies. Furthermore, scintigraphic imaging using <sup>99m</sup>Tc glucarate needs to be studied to determine if this alternative tumour targeting agent can localize in all cell line human breast cancer xenografts, as well as differentiate benign and malignant breast tumours.

FASTSPECT demonstrated the ability to provide high-resolution tomographic images in a mouse model, combined with the capability for fast dynamic SPECT imaging. This novel imaging system allows quantitative

dynamic imaging and functional determination of radio-tracer kinetics in mice with xenografted tumours.

## Acknowledgements

The authors wish to acknowledge Bethany Skovan, Gillian Paine and Henry Allan Toppin for assistance in establishing the animal tumour models, and Brenda K. Baggett for her expertise in preparing tissues for western blotting.

## References

- Maublant J. Scintigraphic imaging of breast tumors. *Eur J Radiology* 1997; **24**:2-10.
- Buscombe JR, Cwikla JB, Thakrar DS, Hilson AJ. Scintigraphic imaging of breast cancer: a review. *Nucl Med Commun* 1997; **18**:698-709.
- Khalkhali I, Villanueva-Meyer J, Edell SL, Connolly JL, Schnitt SJ, Baum JK, et al. Diagnostic accuracy of <sup>99m</sup>Tc-sestamibi breast imaging: multicenter trial results. *J Nucl Med* 2000; **41**:1973-1979.
- Bennink RJ, Rijks LJ, van Tienhoven G, Noorduy LA, Janssen AG, Sloof GW. Estrogen receptor status in primary breast cancer: iodine 123-labeled cis-11beta-methoxy-17alpha-iodovinyl estradiol scintigraphy. *Radiology* 2001; **220**:774-779.
- Ivanovic V, Wolter A, Winzer K, Aldinger H, Muller JM, Munz DL. Intraindividual comparison of F-18-fluorodeoxyglucose and Tc-99m-tetrofosmin in planar scintimammography and SPECT. *Clin Positron Imaging* 2000; **3**:17-29.
- Berghammer P, Obwegeser R, Mulauer-Ertl S, Karanikas G, Wiltschke C, Kubista E, et al. 99m-Tc-tetrofosmin scintigraphy and breast cancer. *Gynecol Oncol* 1999; **73**:87-90.
- Petrov AD, Narula J, Nakazawa A, Pak KY, Khaw BA. Targeting human breast tumor in xeno-grafted SCID mice with <sup>99</sup>Tc<sup>m</sup>-glucarate. *Nucl Med Commun* 1997; **18**:241-251.
- Mariani G, Molea N, Lazzeri E et al. A pilot clinical trial on scintimammography (SMM) with <sup>99m</sup>Tc-D-glucaric acid in patients with breast cancer [Abstract]. *J Nucl Med* 2002; **43**(suppl):288p.
- Khalkhali I, Baum JK, Villanueva-Meyer J, Edell SL, Hanelin LG, Lugo CE, et al. (99m)Tc sestamibi breast imaging for the examination of patients with dense and fatty breasts: multicenter study. *Radiology* 2002; **222**:149-155.
- Jackson VP, Henrick RE, Feig SA, Kopans DB. Imaging of the radiographically dense breast. *Radiology* 1993; **188**:297-301.
- Krishnaiah G, Sher-Ahmed A, Ugwu-Dike M, Regan P, Singer J, Totoonchie A, et al. Technetium-99m sestamibi scintimammography complements mammography in the detection of breast cancer. *Breast J* 2003; **9**:288-294.
- Alonso O, Massardo T, Delgado LB, Horvath J, Kabasakal L, Llamas-Olier A, et al. Is (99m)Tc-sestamibi scintimammography complementary to conventional mammography for detecting breast cancer in patients with palpable masses? *J Nucl Med* 2001; **42**:1614-1621.
- Riordan JR, Deuchars K, Kartner N, Alon N, Trent J, Ling V. Amplification of P-glycoprotein genes in multidrug-resistant mammalian cell lines. *Nature* 1983; **316**:817-819.
- Hamada H, Tsuruo I. Functional role for the 170- to 180-kDa glycoprotein specific to drug-resistant tumor cells as revealed by monoclonal antibodies. *Proc Natl Acad Sci USA* 1986; **83**:7785-7789.
- Piwonica-Worms D, Chiu ML, Budding M, Kronauge JF, Kramer RA, Croop JM. Functional imaging of multidrug-resistant P-glycoprotein with an organotechnetium complex. *Cancer Res* 1993; **53**:977-984.
- Rao VV, Chiu ML, Kronauge JF, Piwonica-Worms D. Expression of recombinant human multidrug resistance P-glycoprotein in insect cells confers decreased accumulation of technetium-99m-sestamibi. *J Nucl Med* 1994; **35**:510-515.
- Del Vecchio S, Ciarmiello A, Pace L, Potena MI, Carriero MV, Mainolfi C, et al. Fractional retention of technetium-99m-sestamibi as an index of P-glycoprotein expression in untreated breast cancer patients. *J Nucl Med* 1997; **38**:1348-1351.
- Columbi A, Maroni M, Antonini C, Fait A, Zocchetti C, Foà V. Influence of sex, age and smoking habits on urinary excretion of D-glucaric acid. *Clin Chim Acta* 1983; **128**:349-358.
- Orlandi C, Crane PD, Edwards S, Platts SH, Bernard L, Lazewatsky J, et al. Early scintigraphic detection of experimental myocardial infarction in dogs with <sup>99m</sup>Tc glucaric acid. *J Nucl Med* 1991; **32**:263-268.
- Yaoita H, Uehara T, Brownell AL, Rabito CA, Ahmad M, Khaw BA, et al. Localization of technetium-99m-glucarate in zones of acute cerebral injury. *J Nucl Med* 1991; **32**:272-278.
- Narula J, Petrov A, Pak KY, Lister BC, Khaw BA. Very early noninvasive detection of acute experimental nonreperfused myocardial infarction with <sup>99m</sup>Tc-labeled glucarate. *Circulation* 1997; **95**:1577-1584.
- Molea N, Lazzeri E, Bodei L, Bacciardi D, Khaw BA, Pak KY, et al. Biodistribution pharmacokinetics and dosimetry of <sup>99m</sup>Tc-D-glucaric acid in humans. In: (editor). *Clinical Medicine and Research XXII*. Basel, Switzerland: Birkhäuser Verlag; 1997, pp. 359-364.
- Taylor CW, Dalton WS, Parrish PR, Gleason MC, Bellamy WT, Thompson FH. Different mechanisms of decreased drug accumulation in doxorubicin and mitoxantrone resistant variants of the MCF7 human breast cancer cell line. *Br J Cancer* 1991; **63**:923-929.
- Klein WP, Barrett HH, Pang IW, Patton DD, Rogulski MM, Sain JD, et al. FASTSPECT: Electrical and mechanical design of a high-resolution dynamic SPECT imager. Conference Record of the 1995 IEEE Nuclear Science Symposium and Medical Imaging, San Francisco, CA 1995; **2**:931-933.
- Kastis GK, Barber HB, Barrett HH, Giggord HC, Pang IW, Patton DD, et al. High resolution SPECT imager for three-dimensional imaging of small animals [Abstract]. *J Nucl Med* 1998; **39**(suppl):9P.
- Delmon-Moingeon LI, Piwonica-Worms D, Van den Abbeele AD, Holman BL, Davison A, Jones AG. Uptake of the cation hexakis(2-methoxyisobutylisocyanide)-technetium-99m by human carcinoma cell lines *in vitro*. *Cancer Res* 1990; **50**:2198-2202.
- Chiu ML, Kronauge JF, Piwonica-Worms D. Effect of mitochondrial and plasma membrane potentials on accumulation of hexakis (2-methoxyisobutylisocyanide) technetium(I) in cultured mouse fibroblasts. *J Nucl Med* 1990; **31**:1646-1653.
- Carvalho PA, Chiu ML, Kronauge JF, Kawamura M, Jones AG, Holman BL, Piwonica-Worms D. Subcellular distribution and analysis of technetium-99m-MIBI in isolated perfused rat hearts. *J Nucl Med* 1992; **33**:1516-1522.
- Piwonica-Worms D, Kronauge JF, Delmon L, Holman BL, Marsh JD, Jones AG. Effect of metabolic inhibition on technetium-99m-MIBI kinetics in cultured chick myocardial cells. *J Nucl Med* 1990; **31**:464-472.
- ten Kate CI, Fishman AJ, Wilkinson RA. Tc-99m-glucaric acid: A glucose analogue [Abstract]. *Eur J Nucl Med* 1990; **17**:451.
- Webb TE, Pham-Nguyen MH, Darby M, Hamme AT. Pharmacokinetics relevant to the anti-carcinogenic and anti-tumor activities of glucarate and the synergistic combination of glucarate:retinoid in the rat. *Biochem Pharmacol* 1994; **47**:1655-1660.
- Abou-Issa H, Dwivedi C, Curley RW, Kirkpatrick R, Koolemans-Beynen A, Engineer FN, et al. Basis for the anti-tumor and chemopreventive activities of glucarate and the glucarate:retinoid combination. *Anticancer Res* 1993; **13**:395-399.
- Maurer AH, Caroline DF, Jadali FJ, Manzone TA, Maier WP, Au FC, et al. Limitations of craniocaudal thallium-201 and technetium-99m-sestamibi mammoscintigraphy. *J Nucl Med* 1995; **36**:1696-1700.
- Khalkhali I, Cutrone J, Mena I, Diggles L, Venegas R, Vargas H, et al. Technetium-99m-sestamibi scintimammography of breast lesions: clinical and pathological follow-up. *J Nucl Med* 1995; **36**:1784-1789.
- Yutani K, Shiba E, Kusuoka H, Tatsumi M, Uehara T, Taguchi T, et al. Comparison of FDG-PET with MIBI-SPECT in the detection of breast cancer and axillary lymph node metastasis. *J Comput Assist Tomogr* 2000; **24**:274-280.